Sensitivity of Simulated Global Climate to Perturbations in Low Cloud Microphysical Properties. Part II: Spatially Localized Perturbations

C.-T. CHEN† AND V. RAMASWAMY*

Atmospheric and Oceanic Sciences Program, Princeton University, Princeton, New Jersey

(Manuscript received 9 October 1995, in final form 10 April 1996)

ABSTRACT

The sensitivity of the global climate to spatially localized (20°–70°N) perturbations in the microphysical properties of low clouds is investigated using a general circulation model coupled to a mixed layer ocean with fixed cloud distributions. By comparing with earlier experiments involving globally uniform perturbations, insights are obtained into the climate responses to spatially inhomogeneous radiative forcings, such as that due to the contrast in the effective drop radius of land and ocean clouds and the anthropogenic sulfate aerosol-induced alteration of cloud albedo. The main findings of this study are as follows: 1) The model's climate sensitivity (ratio of global-mean surface temperature response to the global-mean radiative forcing) is virtually independent of the distribution and magnitude of forcing. 2) Although the total feedback is very similar in the different experiments, the strengths of the individual feedback mechanisms (water vapor, albedo, lapse rate) are dissimilar. 3) For the localized perturbations, the climate response is essentially confined to the hemisphere in which the forcing occurs, owing to a poor interhemispheric energy exchange. 4) In spite of no forcing in the Southern Hemisphere in the localized experiments, there is a weak "remote" temperature response there. 5) For both global and localized perturbations, the temperature response in the tropical upper troposphere is larger than in the lower troposphere due to moist convective processes; in the localized experiments, while there is a strong vertical gradient in the temperature change at the Northern Hemisphere mid and high latitudes, the temperature change throughout the lower and midtroposphere of the Southern Hemisphere is uniform. 6) The localized experiments induce notable changes in the mean meridional circulation and precipitation near the equator, which are not obtained for the global perturbation cases. 7) The pattern of temperature response of the land and ocean areas in the Northern Hemisphere midlatitudes depends on whether the forcing occurs over both types of surfaces or over land only; the results suggest that the well-known contrast in drop radii between continental and maritime clouds exerts a significant influence on the surface temperature distribution within the zone and on the manner in which the surface energy balance is maintained.

1. Introduction

It is well known that differences or changes in water drop concentrations and sizes introduce variations in the solar radiative properties of clouds (Charlson et al. 1987; Slingo 1989) and, because of the importance of clouds in the climate system (IPCC 1992), are issues of substantial climatic importance. An example of differences in microphysics is that revealed by observations made in continental and maritime clouds (Squires 1958; Twomey and Wojciechowski 1969).

An example of change in cloud microphysics is that potentially induced by anthropogenic causes (Twomey 1977). Cloud drop characteristics are related to cloud condensational nuclei or CCN (Twomey and Squires 1959; Hudson 1984), and an important source of the CCNs is sulfate aerosols resulting from sulfur emissions due to fossil fuel combustion (Schwartz 1988). Approximately 76% of the anthropogenic sulfur gases is emitted in the 20°–70°N belt (Spiro et al. 1992), which results in the sulfate aerosols being distributed primarily in the Northern Hemisphere midlatitudes (Langner et al. 1992). Increases in CCN and thus cloud drop concentrations caused by the anthropogenic aerosols have the potential to increase the albedo of the planet and thus to some extent counteract the enhanced greenhouse effect due to increases in trace gases (Twomey et al. 1984; Charlson et al. 1992). Further, the anthropogenic aerosols yield a relatively more spatially inhomogeneous pattern of forcing in the midlatitude Northern Hemisphere compared to greenhouse gas increases (IPCC 1994). While the connection between changes in aerosols and CCN and the resulting perturbations in cloud albedo is recognized as being physically plausible, there remain major uncertainties in quantifying the spatial and seasonal dependence of the relationship between SO_2 emissions, CCN concen-

* Also affiliated with NOAA/Geophysical Fluid Dynamics Laboratory, Princeton University, Princeton, New Jersey.

† Current affiliation: Department of Earth Sciences, National Taiwan Normal University, Taipei, Taiwan.

Corresponding author address: Dr. V. Ramaswamy, NOAA/GFDL, Princeton University, Princeton, NJ 08542.

trations, cloud drop concentrations, and cloud optical properties (Penner et al. 1994). This limits the ability to characterize accurately the spatio–temporal changes in the aerosol and cloud drop properties.

Motivated by the above, we employ a general circulation model (GCM) in this study to obtain insights into the sensitivity of the climatic impacts due to the observed difference in the land and marine cloud microphysics and that due to potential changes in cloud microphysics in the Northern Hemisphere. To carry out the study, we prescribe and perturb the cloud microphysical properties in a simple manner. Specifically, we adopt an idealized description of the geographical distribution of cloud microphysical properties and impose an idealized specification of changes. Further, we restrict the perturbations in cloud microphysics to low clouds only, which are more likely to be affected by the anthropogenic aerosols.

This paper and its objectives constitute a companion study to Chen and Ramaswamy (1996, hereafter CR96), and the strategy of the investigation is similar, except we now consider spatially localized (Northern Hemisphere midlatitude) instead of globally uniform perturbations in the low cloud microphysics. Recapitulating one of the results in CR96, we illustrated there that the climate sensitivity (i.e., global mean temperature change divided by global mean forcing) is virtually the same irrespective of the sign and magnitude of radiative forcing caused by changes in cloud microphysical properties; further, the sensitivity is the same as for doubling of CO_2. In this paper, we pose the following questions concerning climate sensitivity: (i) whether there is any difference in the sensitivity if the change in cloud radiative properties is applied locally as opposed to globally; and (ii) whether the contrast in the microphysical properties of clouds over land and ocean, as, for example, understood to exist between continental and maritime clouds, lead to differences in model simulations of climate.

Two GCM experiments are undertaken to investigate these issues. As in CR96, the cloud amounts and distributions are held fixed during the model integrations so that there are no cloud-related feedbacks. By imposing a change in the cloud microphysical properties and holding them fixed, the perturbations considered here can be assumed to be external forcings. As in CR96, these solar forcings amount to changes in the albedo of the surface–atmosphere system.

The radiative transfer algorithm follows Chen and Ramaswamy (1995, hereafter CR95), while the simulation of the "control" climate is discussed in CR96. In section 2, the perturbation experiments and radiative forcing are discussed. For each experiment, the annual-mean thermal and dynamical (section 3) and hydrological (section 4) responses are analyzed. The manner in which the terms in the surface energy budget are altered is discussed in section 5, while the climate feedback processes are analyzed in section 6. Section 7 summarizes the major findings.

2. Model and the formulation of GCM experiments

a. *Description of the model and "control" simulation*

The climate model is an R15 nine-level global atmospheric GCM coupled to a simple model of the oceanic mixed layer (CR96). The process of sea ice formation is explicitly incorporated, but the effect of heat transport by ocean currents is not included. The seasonal cycle of insolation is prescribed at the top of the atmosphere, but the diurnal variation is not included. As in CR96, zonally uniform and seasonally invariant cloud cover (see the Fixed Cloud model of Manabe and Broccoli 1985) is prescribed with respect to latitude and height. The latitudinal distribution of low cloud cover is shown in Ramaswamy and Chen (1993, hereafter RC; their Fig. 3). It is reiterated that, as in CR96, cloud-related feedbacks are not considered.

For simplicity, the drop effective radius in the control is assumed to be 10 μm for all clouds. The LWPs for high and middle clouds are fixed at 7 and 25 g m^2, respectively, while the nominal value assigned to the low clouds is 80 g m^{-2}. For the low cloud, the choice of LWP and r_e yields an optical depth of 12.7, approximately consistent with inferences from satellite observations (Rossow and Lacis 1990).

The surface temperatures simulated by the model are quite close to the observed values throughout the tropical and midlatitude regions in both hemispheres (CR96). Poleward of 55°, the model temperatures are somewhat too warm, particularly in the Antarctic region. The model succeeds in reproducing the extensive rainfall in the Tropics; however, the precipitation rate in the simulation is overestimated at the high latitudes. The overall performance of this model in simulating the present climate is reasonable and offers a convenient basis for doing idealized climate perturbation experiments.

b. *Formulation of the experiments*

The climate sensitivity to spatially localized albedo perturbations is investigated through two idealized experiments (Table 1), with the forcings computed as in CR96. Each experiment consists in perturbing a low-cloud microphysical property from its value in the "control" run. The localized perturbations consist of

(i) 100% increase in LWP in the 20°–70°N belt (Localized Liquid Water Increase Experiment, designated as LLI);

(ii) 28% decrease in r_e over continental areas in the 20°–70°N belt (Localized Land–Marine Contrast Experiment, designated as LCM).

TABLE 1. GCM experiments for studying the sensitivity of the model climate to changes in low-cloud microphysical properties. The nominal values for low cloud liquid water path (LWP) and effective radius are 80 g m^{-2} and 10 μm and are uniform throughout the globe. The LLI and LCM experiments are discussed in section 2b while GLI/2 is discussed in CR96.

Experiment	Perturbation in low cloud	Perturbation domain	Global and annual mean radiative forcing (W m^{-2})
LLI	100% increase in LWP	20°–70°N	−1.9
LCM	28% decrease in effective radius	land area between 20°–70°N	−0.8
GLI/2	17% increase in LWP	global	−1.9

For a comparison with the global perturbations in CR96, we refer to one of the cases in that study, namely, the "GLI/2" perturbation, which consisted of a 17% globally uniform increase in low cloud LWP (Table 1). Thus, GLI/2 and LLI contrast the effects of localized and global albedo perturbations, keeping the globally averaged forcing the same, equal to approximately one-half of that due to a doubling of carbon dioxide. The LLI experiment serves to illustrate the effects due to an increase of cloud albedo and, more generally, the planetary albedo in the Northern Hemisphere midlatitudes. This experiment bears relevance to the climate issue raised by Charlson et al. (1991) that the Northern Hemisphere midlatitude albedo ("direct" and "indirect" forcing; IPCC 1994) may have increased since preindustrial times due to increase in anthropogenic sulfate aerosols. We emphasize, however, that the present study is not an attempt to determine the actual effects due to sulfate aerosols. Instead, the aim is to investigate the climate sensitivity to a spatially inhomogeneous forcing, an example of which is that due to the anthropogenic sulfate aerosols. Although we perturb cloud LWP, there is a near-equivalence in the climatic effects whether LWP or r_e is changed (CR96). Note also that a cloud with smaller drops could rain less and thus enhance the LWP.

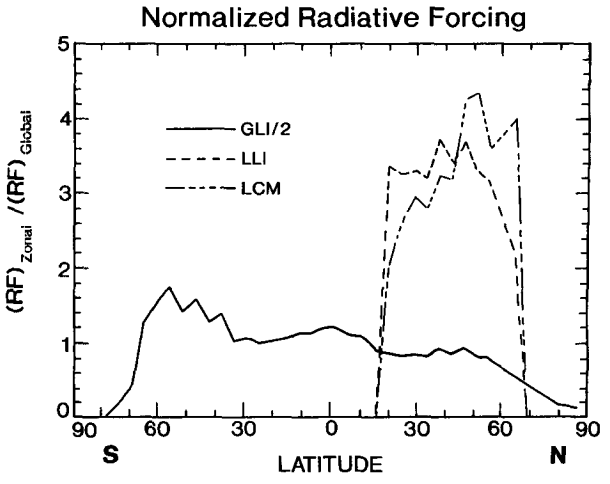

FIG. 1. Annual-mean "normalized" (zonal mean divided by global mean) radiative forcing in the LLI, LCM, and GLI/2 experiments.

One motivation for the LCM experiment is to investigate the effect of the contrast in the drop sizes of continental and maritime clouds. The r_e of continental low clouds is reduced by 28% (from 10 to 7.2 μm) following Han et al. (1994), while the r_e over oceans remains at 10 μm. The nature of the LCM perturbation is similar in concept to that reported in Kiehl (1994). This experiment, too, has relevance to the aerosol climate issue posed in Charlson et al. (1991). They estimate the albedo changes due to the direct effect of sulfate aerosols to occur over the Northern Hemisphere midlatitude continental areas. Thus, by restricting a perturbation to the 20°–70°N continental regions of Northern Hemisphere in LCM, the response to an albedo increase occurring only over the polluted midlatitude land areas may be evaluated. Hence, the comparison of the LCM experiment with the control run allows the exploration of two different sensitivity issues: (i) the consequence of a difference in the cloud microphysical properties of continental and maritime environments, and (ii) the consequence of a Northern Hemisphere, continental-area only, aerosol effect. The magnitude of the global-mean radiative forcing in LCM is less than LLI since only the clouds over land are perturbed.

We note that while the area of the LLI perturbation is comparable in extent to the Northern Hemisphere midlatitude 'indirect' aerosol forcing in Jones et al. (1994), the extent in LCM is an idealization of the essentially continental forcing in Erickson et al. (1995). As in CR96, a substantial period of integration (~25 years) was required in order to reach a new equilibrium climate for each experiment. Each simulation was then continued for an additional 10 years, and the averages of the climate variables over the last 10 years are taken to be the equilibrium responses.

c. *Zonal mean solar radiative forcing*

Figure 1 shows the "normalized" forcing (zonal mean divided by global mean) in LLI, LCM, and GLI/2. This plot highlights the relative latitudinal distribution of the forcing. A relatively stronger forcing (almost twice as large as the global and annual mean) for the GLI/2 experiment occurs near 60°S where the cloud amount is highest (see RC). When a forcing is applied only between 20° and 70°N (LLI and LCM),

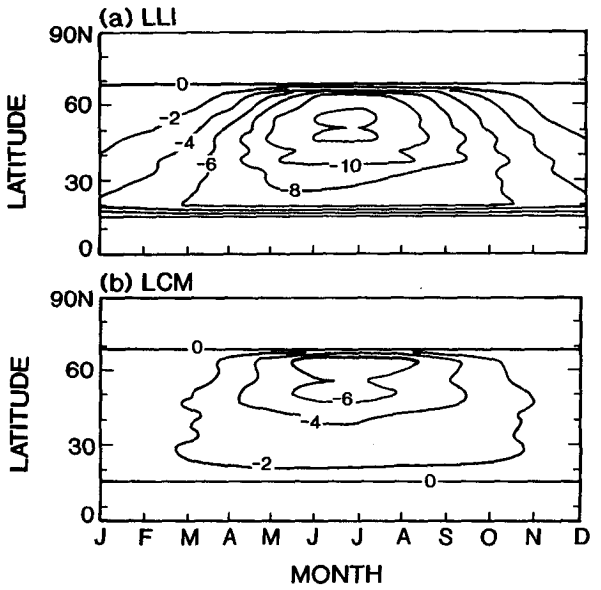

FIG. 2. Zonal, monthly mean distribution of radiative forcing (W m^{-2}) in the (a) LLI and (b) LCM experiments.

the normalized zonal values have a peak more than three times as large as the global mean. Compared to LLI, the land-area distribution between 45° and 70°N and the presence of larger cloud amounts at the higher latitudes results in a relatively stronger forcing there and a poleward shift of the peak in LCM.

In LLI, the zonal mean radiative forcing can be as large as -12 W m^{-2} during summer owing to the large insolation available at that time (Fig. 2a). The absolute magnitude of the global mean forcing (-0.8 W m^{-2}, Table 1) in LCM is less than in LLI; however, the amplitude of the zonal mean forcing during summer over the land + ocean areas can still be as large as 7 W m^{-2} (Fig. 2b). Relative to LLI, the domain of peak values in LCM is shifted slightly poleward. It may be noted that the ratio of r_e between continental and maritime clouds observed in some measurements raises the possibility of an even larger contrast [0.46 from Squires (1958) in contrast to 0.72 here]; this would yield a larger radiative forcing over continents.

3. Thermal response

First we discuss the response in the LLI experiment. The zonal surface temperature response in LLI is essentially confined to the Northern Hemisphere (Fig. 3). A polar amplification of the surface temperature response is found in the Northern Hemisphere despite the fact that there is no forcing beyond 70°N (Fig. 1). The physical mechanisms responsible for this are essentially similar to those in the case of the CO_2-increase simulations (Manabe and Stouffer 1980), namely, changes in the amount and thickness of sea ice accompanied by changes in the polar surface albedo and the stable stratification of the lower troposphere at the higher latitudes. Figure 4a illustrates the distributions of the zonal, annual-mean changes in surface-air temperature, while Fig. 4b shows the change in surface albedo. The advancement and thickening of sea ice due to the negative forcing is accompanied by a larger surface albedo at the higher latitudes, which further reduces the net solar flux absorbed. The alteration of the

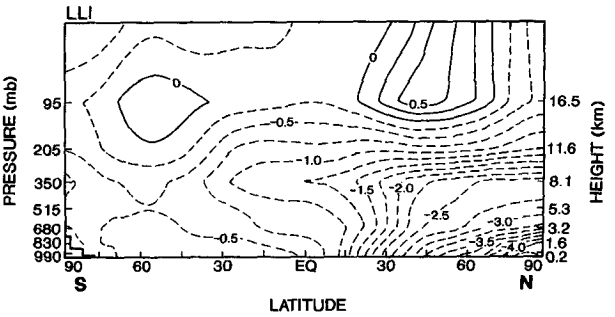

FIG. 3. Latitude–height distribution of the changes in zonal, annual-mean temperature (K) in the LLI experiment.

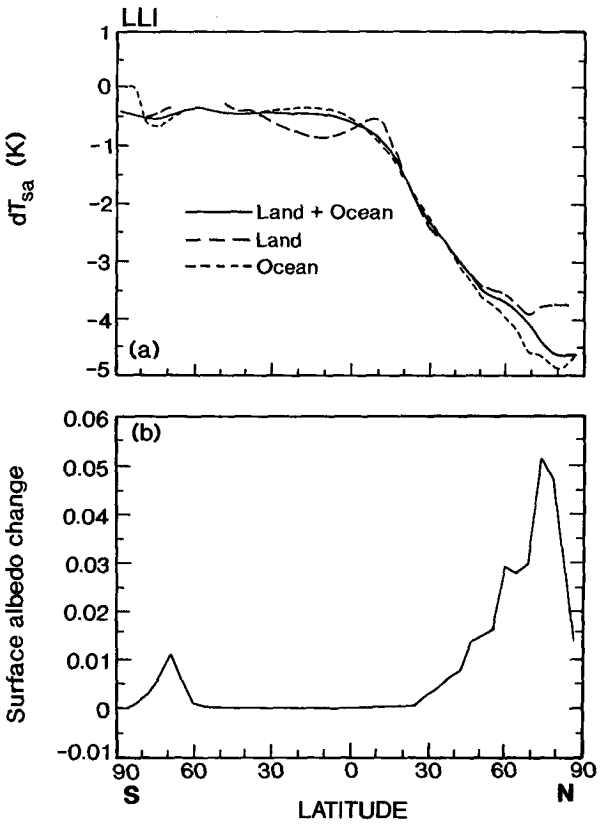

FIG. 4. Zonal, annual-mean distribution of the changes in the (a) land-only, ocean-only, and land + ocean surface-air temperatures (K) and (b) surface albedo in the LLI experiment.

TABLE 2. Changes in annually averaged global-mean surface air temperature (T_s) and precipitation (P) in the LLI, LCM, and GLI/2 experiments. The values of T_s and P in the control run and the radiative forcing in each experiment are also listed.

	ΔT_s (K)	ΔP (cm yr^{-1})	Forcing (W m^{-2})
LLI	−1.4	−3.9	−1.9
LCM	−0.6	−1.0	−0.8
GLI/2	−1.4	−4.1	−1.9
		T_s (K)	P (cm yr^{-1})
Control run		288.5	109.1

sea ice amount and thickness (and, thereby, its thermal insulation effect) varies with season. Further, the greater stability of the atmosphere near the surface in the high latitudes tends to concentrate the cooling at the lower altitudes. There results, thus, a relatively larger decrease of the surface air temperature at the higher latitudes. The zonal-mean temperature responses for land and ocean areas separately are also shown in Fig. 4a. The differences in the temperature change in the Arctic region between land and sea are attributable to the changes in sea ice mentioned above and to the differences in the surface albedo change, respectively, between continental and oceanic areas. In the Tropics, despite the absence of any initial forcing, there is a land-surface temperature response, owing to changes in circulation and hydrologic parameters (this will be discussed later).

In both the land and oceanic areas of the Southern Hemisphere, the zonal mean surface temperature decreases by slightly less than 0.5 K (Fig. 3). This has to be considered a "remote" response since the forcing is only in the Northern Hemisphere. This response, however, is much less compared to that in the Northern Hemisphere mid- and high latitudes. The large difference in the hemispheric temperature responses suggests that, in the model, the radiative–dynamical compensation within the Northern Hemisphere to the applied forcing is much more effective than an advective adjustment involving cross-hemispheric heat exchange. Such a feature was also found in a model study of the effect of continental ice sheets (Manabe and Broccoli 1985). Figure 3 also shows that a strong vertical gradient in the temperature change occurs in the mid- to high latitudes of the Northern Hemisphere where the forcing is applied, indicating sharp changes in the local lapse rate. In contrast, the smaller temperature response in the Southern Hemisphere, a remote effect, is rather uniform throughout the low and midtroposphere.

Comparing LLI with GLI/2 (see CR96), the different latitudinal distribution of the radiative forcing in the two cases leads to distinctly different temperature response patterns, including the Northern Hemisphere. However, from Table 2, the ratio of the globally, annually averaged temperature response to the globally, annually averaged radiative forcing is approximately similar for these two cases.

The interhemispheric difference in the responses (Fig. 4) yields an enhanced temperature gradient between the two hemispheres and induces a change in the zonal mean meridional circulation between 20°N and 20°S. Figure 5a shows the change in the annually averaged zonal mean meridional mass streamfunction, while Fig. 5b shows the control state. The tendency for surface cooling reduces convective activity and thereby the diabatic (mainly latent) heating of the atmosphere in the Northern Hemisphere tropical region (Fig. 5c). The change in the zonal mean meridional circulation intensifies somewhat the heat and moisture exchange between the two hemispheres near the equator.

Between 0° and 20°S, there is a strengthening of the ascending branch of the mean meridional circulation;

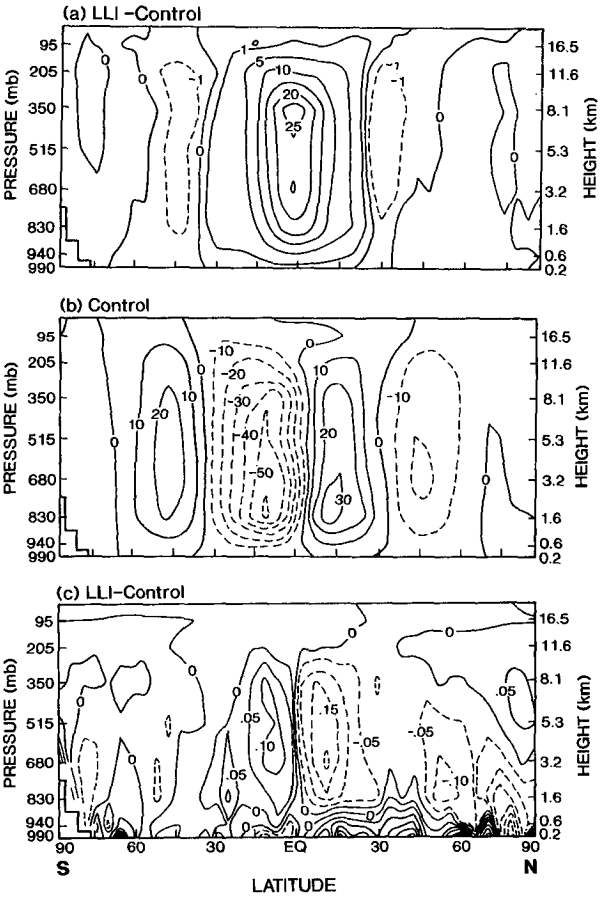

FIG. 5. (a) Change in the annually averaged zonal-mean meridional mass streamfunction in the LLI experiment and (b) the value in the "control" climate. Solid (positive values) and dashed (negative values) contours indicate clockwise and anticlockwise circulations, respectively (units: 10^9 kg s^{-1}). The maximum value in a cell is an indication of the strength of the mass transport by that cell. (c) Latitude–height distribution of the zonal-mean change in the diabatic heating (K d^{-1}) in the LLI experiment.

this is accompanied by a strong moisture flux convergence. The same change in the mean meridional circulation discussed above acts to weaken the ascending branch of the meridional circulation in the Northern Hemisphere equatorial region (Fig. 5a). The different temperature responses of the two hemispheres are thus strongly linked to changes in the zonal mean circulation and tropical moisture budget. Such changes in the zonal mean circulation are not present in the global perturbation experiments, for example, GLI/2.

The zonal-mean response pattern for LCM (Fig. 6) is very similar to LLI (Fig. 3), with the change in the global mean surface-air temperature in the LCM experiment slightly less than one-half of LLI (Table 2). The ratio of the responses in these experiments is very similar to what would be anticipated if a linear, invariant relation existed between the global-mean forcing and surface temperature response.

Since the global-mean forcings and, hence, the responses in the two experiments are not the same, we compare their respective normalized responses (Fig. 7) that is, zonal mean divided by the global mean (Table 2). The middle panel of Fig. 7 shows the similarity in the patterns of the land-only surface temperature response at the Northern Hemisphere mid- and high latitudes in the two experiments. Over oceanic regions (bottom panel), compared to the LLI experiment, the normalized zonal temperature reductions in LCM are smaller in the Northern Hemisphere low and midlatitudes but enhanced at the higher latitudes. The features in Figs. 7b and 7c add up to yield the pattern for the total (Fig. 7a). From low to about midlatitudes, the LCM results, compared to LLI, are approximately consistent with the differences in the normalized forcings (Fig. 1), although it must be noted that a one to one correspondence of the differences between LLI and LCM in the normalized forcing and response plots is probably not possible. The high-latitude difference in the normalized temperatures is related to the slightly larger relative change in the ocean surface albedo occurring there for the LCM case (Chen 1994). This is, in turn, related to the peak in the zonal-mean forcing

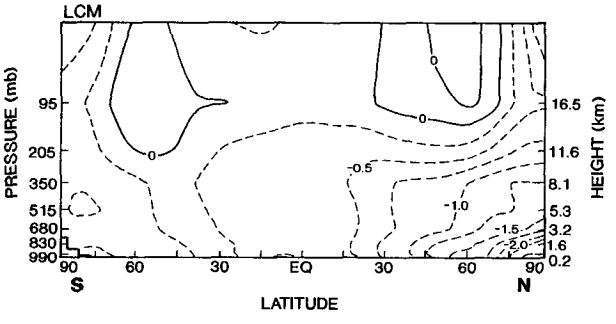

FIG. 6. Latitude–height distribution of the changes in zonal, annual-mean temperature (K) in the LCM experiment.

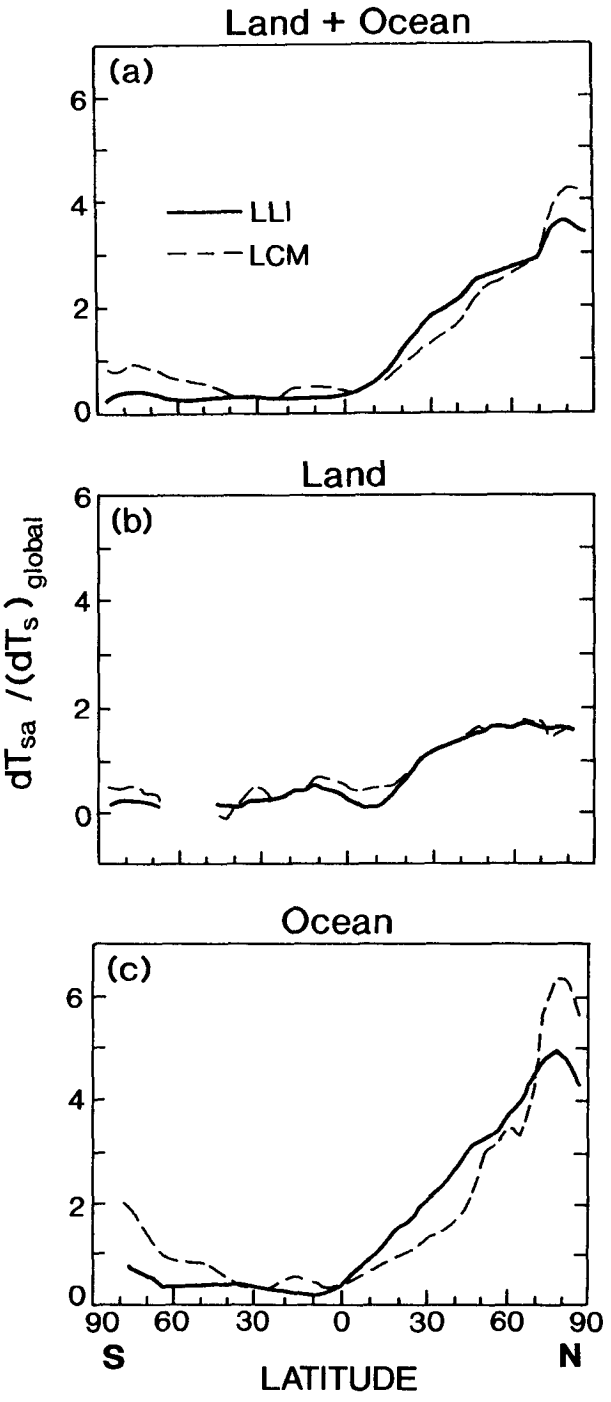

FIG. 7. Annual-mean "normalized" changes (zonal mean divided by global mean) in the (a) land + ocean, (b) land-only, and (c) ocean-only surface-air temperatures in the LLI and LCM experiments.

for the LCM case appearing more poleward than that for LLI and having a slightly larger normalized value (Fig. 1). The normalized high-latitude temperature cooling, relative to the global-mean temperature de-

crease, is larger in LCM (e.g., at 75°N, this ratio is 5.8 in LCM, while it is 4.6 in LLI). However, the signal in LCM is not large enough to assure statistical significance at the high latitudes.

The geographical distribution of the temperature response normalized to the global mean (Fig. 8) shows that the smaller changes in the northern Pacific and northern Atlantic Oceans in LCM relative to LLI (the normalized response is less in LCM from the Tropics to the midlatitudes) are the cause of the lesser midlatitude zonal values in Fig. 7c. This feature is not surprising considering that the radiative forcing in LCM is only over the midlatitude land areas. Comparing the LLI and LCM results, it is seen that the longitudinal asymmetry of the temperature response within the midlatitude domain depends on whether the forcing is zonally uniform or is confined to only the land portions in the zone. The high-latitude geographical regions have a larger normalized response in LCM, which leads to the zonal results in Fig. 7. It is worth mentioning that both LLI and LCM have different patterns of zonal-mean changes compared to the global perturbation experiments (Chen 1994).

4. Hydrologic response

Figure 9a shows the latitude–height cross section of the changes in water vapor mixing ratio in LLI. Corresponding to the temperature response (Fig. 3), the reduction in the water vapor mixing ratio is also mostly confined to the Northern Hemisphere. This is in contrast to the GLI/2 experiment where the changes are global in extent (Fig. 9b). The pattern in LCM (Fig. 9c) is similar to LLI, except the magnitudes are smaller, consistent with the smaller forcing and temperature response.

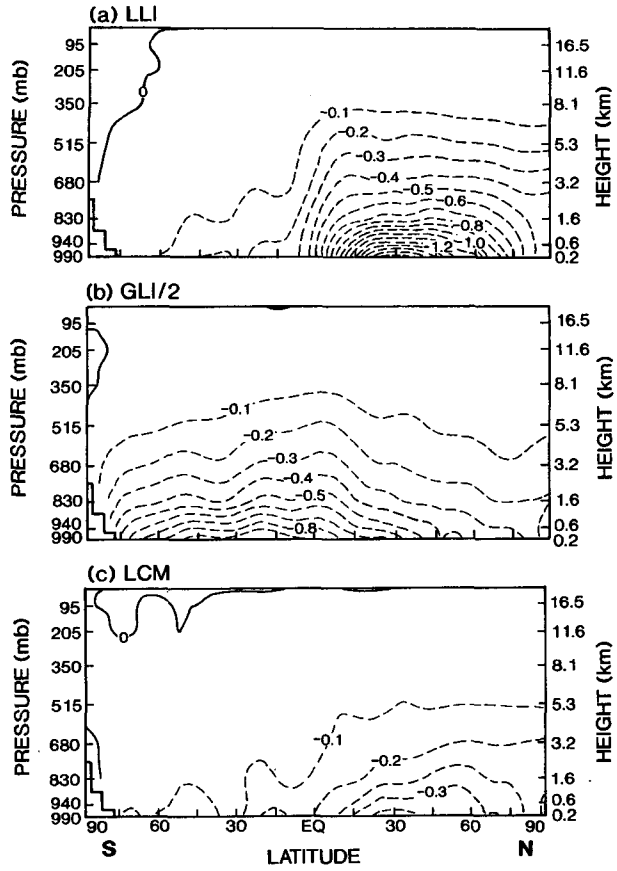

FIG. 9. Latitude–height distribution of the annual-mean changes in the water vapor mixing ratio (g kg^{-1}) in the (a) LLI, (b) GLI/2, and (c) LCM experiments.

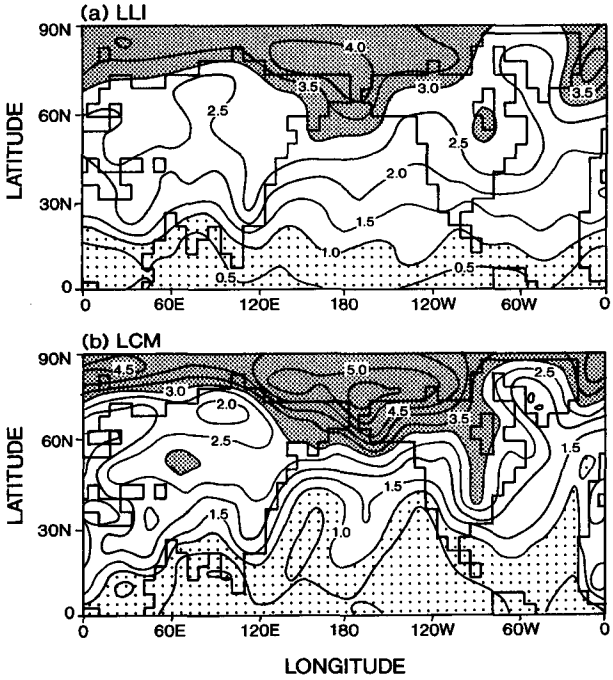

FIG. 8. Geographical distribution of the changes in the annual-mean surface-air temperature, "normalized" with respect to the global, annual-mean change, in the (a) LLI and (b) LCM experiments.

The zonal mean changes in the precipitation rate (P), evaporation rate (E), $P-E$, and soil moisture for LLI are illustrated in Fig. 10. The latitudinal distribution of land-only and the ocean-only averages are also shown in the same figure. In the Northern Hemisphere, decreases in P and E are found in most places accompanying the general decreases in temperature (Fig. 3). The reduction in soil moisture in the Northern Hemisphere equatorial latitudes (0°–10°N) follows roughly the change in P.

As discussed in section 3, a change in the cross-equatorial meridional circulation is induced by the differences in the hemispheric forcing and temperature responses (Figs. 3 and 5a). The increase in P just south of the equator (Fig. 10a) is due to the strong moisture flux convergence accompanying the strengthening of

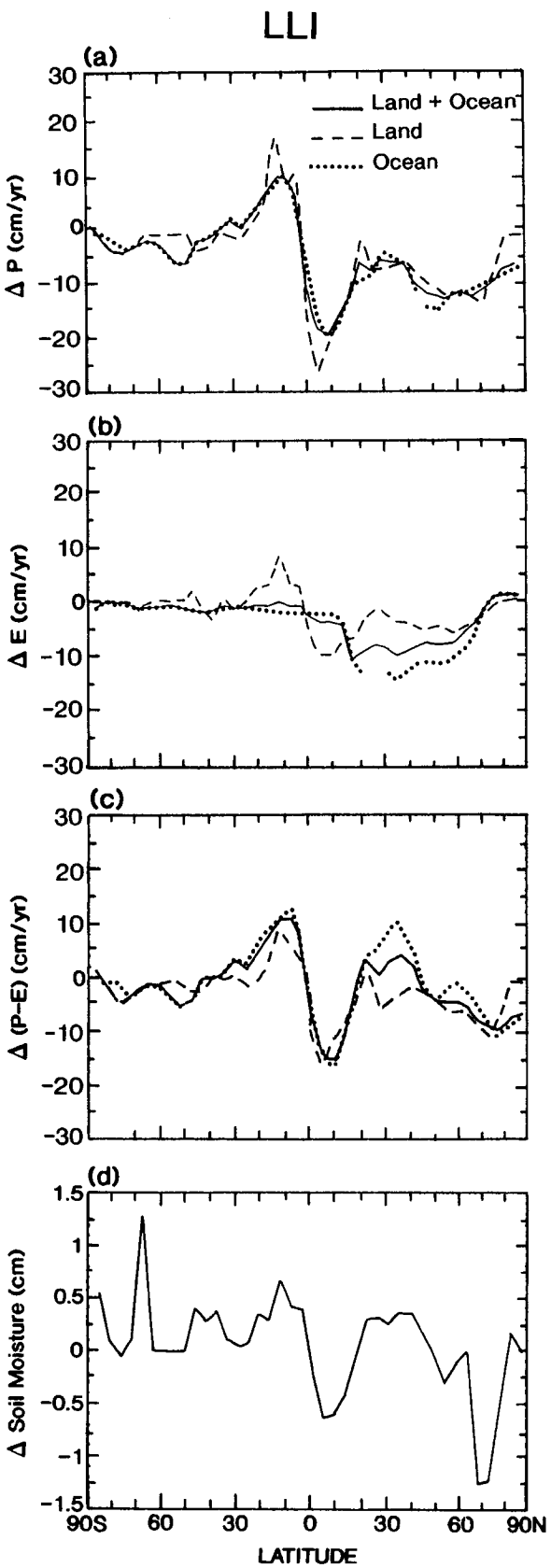

the rising branch of the zonal mean meridional circulation (Fig. 5). In contrast, the weakening of the rising branch of the zonal mean meridional circulation located between the equator and 20°N results in a decrease in P there. The changes in E (Fig. 10b) in the equatorial land region follow the changes in soil moisture (Fig. 10d), which in turn are mainly affected by P (CR95). The magnitude of the change in E for the equatorial land region is smaller than the change in P. This yields a positive $P-E$ between equator and 20°S (Fig. 10c), where the strengthening of the Hadley circulation and an increase in the moisture convergence have occurred. For reasons already stated, a negative $P-E$ occurs between equator and 20°N. Another positive $P-E$ in Northern Hemisphere midlatitude is caused mainly by the reduction in evaporation over the oceans. Despite nearly similar temperature responses over the land and sea areas of the Northern Hemisphere midlatitudes (Fig. 4a), the reduction of E over the oceans is much more than over the continents between 20° and 70°N. The differing surface energy flux balance conditions over oceans and continents (discussed later) is the reason for this feature. Only small changes in sensible heat and longwave radiative fluxes occur over the ocean. Thus, a larger increase in evaporation compensates for the reduction of the solar radiation at the ocean surface.

Over tropical land areas, the surface moisture budget and temperature responses are linked in a distinct manner. In Fig. 10, soil moisture and evaporation over the northern tropical regions are reduced. The dryness and decrease in evaporation, together with the changes in longwave and sensible heat fluxes, tend to lessen the surface cooling initiated by the solar flux change (CR95). The opposite is true in the southern tropical land areas where soil moisture and evaporation increase and the temperature decrease exceeds slightly that in the northern tropical land areas (Fig. 4a).

The zonal mean changes in P, E, $P-E$, and soil moisture in the LCM experiment (see Chen 1994) are qualitatively similar to the LLI results and exhibit the effects to be expected generally from a reduced forcing. The reduction of E over land bears a resemblance to the result in Kiehl (1994). The overall similarity between LLI and LCM points to a robustness in the model's response to localized albedo forcings. The ratio of the global, annual mean changes in P (E) in LCM to LLI is 0.26. It differs from the ratio of the temperature responses for the two experiments (namely, 0.43). This feature is unlike that for global perturbation experiments (e.g., GLI, GLI/2 in CR96), where the relative changes in the global-mean temperature and the precipitation rate were indeed comparable to the

FIG. 10. Zonal, annual-mean distribution of the changes in the (a) precipitation rate (P), (b) evaporation rate (E), (c) $P-E$, and (d) soil moisture in the LLI experiment.

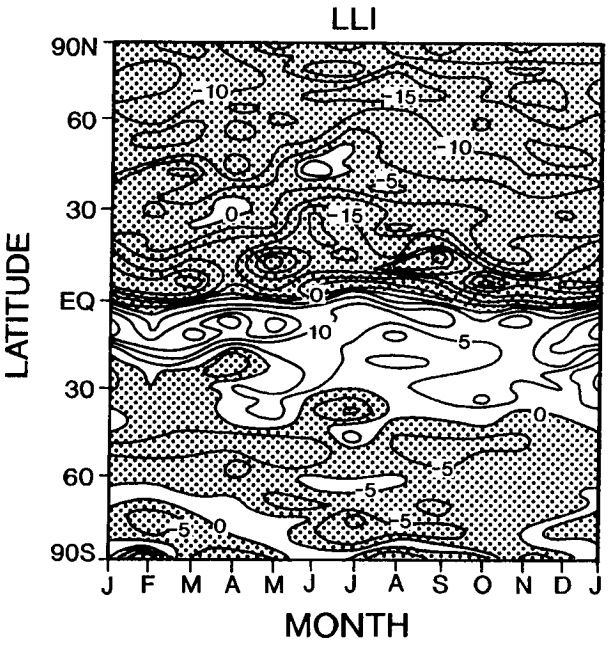

FIG. 11. Latitude–month distribution of the changes in precipitation rate (cm yr^{-1}) in the LLI experiment. Shaded areas denote reduction, while unshaded areas denote increase in precipitation.

ratio of their respective radiative forcings (Table 2 in CR96). A comparison of GLI/2 and LLI experiments reveals that these two have a nearly similar ratio of their respective changes in surface temperature to precipitation rate. Thus, the difference arising for LCM suggests a sensitivity to the zonal asymmetry in a midlatitude forcing.

The prescribed contrast in the continental and maritime cloud properties over the midlatitudes of the Northern Hemisphere (LCM) has a rather peculiar influence on the changes in E. Compared to LLI, there is less of a decrease in E over the northern midlatitude oceans in the LCM experiment; the precipitation changes, too, are less (Chen 1994). From Fig. 9c, it is also evident that the change in water vapor mixing ratio in the LCM experiment is smaller (this is so even if we scale the change with respect to the global-mean radiative forcing). Since there is no solar forcing imposed over the oceans in LCM, there is less of a change required in the surface latent heat flux, and, therefore in the evaporation, for reestablishing the ocean surface energy balance. As pointed out already, because land and ocean areas respond differently to a solar forcing "felt" at the surface, the evaporation changes in LLI for the midlatitude oceanic and land areas are different. For LCM, owing to the forcing occurring only over land, there results less of a difference in E between the land and ocean areas.

The monthly distribution of the changes in P for LLI are negative at almost all locations in the Northern Hemisphere (Fig. 11). On the other hand, strong increases in P are found during all seasons between equator and 20°S. This is related to the changes in the cross-equatorial meridional circulation discussed earlier. The domain with an increase in P extends to 40°S from May through November. The response in the LCM case (see Chen 1994) is similar but is smaller than in LLI due to the weaker forcing, and the changes in P are less well organized. The sharp contrast of P near the equator for LLI is not found for GLI/2. This is in contrast to the similarity of their globally and annually averaged changes (Table 2). An important inference is that although the global-mean surface temperature response and the radiative forcing have the same ratio in LLI and LCM, not all the processes (e.g., global-mean precipitation rate in LCM) can be expected to follow a similar simple linear scaling with respect to the global-mean forcing.

5. Maintenance of the surface energy budget

Following Boer (1993), we investigate the changes in the surface energy budget occurring in the LLI and LCM experiments. By decomposing the changes in the various terms of surface energy budget in the manner described in CR96, we isolate the effects due to various factors. Table 3 lists the global average changes in the various terms, with the terminology being the same as in CR96. Positive values imply a change acting to warm the surface (increased gain or decreased loss), while a negative value implies a change acting to cool the surface.

In response to the initial radiative forcing (Figs. 1 and 2 and Table 2), the new balance of the globally and annually averaged surface energy budget in LLI comes about mainly due to a decrease of latent heat flux output (LE) and a reduction in the net radiation input, with the change in sensible heat (H) being small. The reduction of solar flux input (S) is larger than the decrease of the longwave output (F). The drier atmo-

TABLE 3. Changes (W m^{-2}) in the terms comprising the global- and annual-mean surface energy budget in the LLI, LCM, and GLI/2 experiments. The "control" values are also listed. Here T_{sfc} denotes surface temperature.

		δX in the experiments		
X	Control	LLI	LCM	GLI/2
S	168.9	−1.9	−0.6	−1.8
F	−62.8	−1.2	−0.3	−1.2
LE	−86.5	3.1	0.8	3.2
H	−15.0	0.0	0.2	−0.2
W_{clr}	−86.1	2.0	0.9	1.2
C_{SW}	−63.1	−2.8	−1.0	−2.3
A_{sfc}	−25.9	−1.0	−0.5	−0.7
G_{clr}	320.4	−9.4	−3.9	−9.2
C_{LW}	28.4	0.8	0.3	0.8
σT^4_{sfc}	−411.6	7.4	3.3	7.2

sphere in the new balance (Fig. 9) leads to an increase in the incident solar flux at the surface under clear skies (W_{clr}), but clouds (C_{SW}) act to reduce the solar flux. The surface albedo change effect, A_{sfc}, yields a slightly larger reduction of solar flux than the atmospheric contribution. The large downward longwave flux reduction due to the drier and cooler atmosphere, as evidenced by the decrease in clear-sky contribution G_{clr} (the overcast-sky component, C_{LW}, is much smaller), exceeds the gain due to the reduction of temperature and surface emission, σT_{sfc}^4.

All the terms in the LCM case have the same sign as in LLI but are smaller, consistent with the lesser forcing. In LCM, the latent heat flux change is reduced to about one-fourth of that in LLI (similar to precipitation; Table 2). This reduction is consistent with the result of Kiehl (1994). The effect due to surface albedo changes (A_{sfc}) becomes the dominant contributor to the solar flux change at the surface, with the effects due to clear sky (W_{clr}) and clouds (C_{SW}) canceling out each other.

Figure 12 illustrates the latitudinal dependence of the changes in surface latent heat, sensible heat, and net radiative fluxes for the LLI experiment. Several distinct features are found over the different regions. (i) In the land area between 20° and 70°N, the surface energy reequilibration involves a balance of the radiative term by the sensible and, to a lesser degree, the latent heat fluxes. (ii) The ocean area between 20° and 70°N, on the other hand, has radiative and latent heat fluxes as the dominant terms to arrive at a new balance. (iii) In the tropical land regions of both hemispheres, the changes in sensible heat and radiative fluxes act in the same direction and counteract the changes in the latent heat flux. (iv) Over tropical oceans and in the mid- and high latitudes of Southern Hemisphere, the changes in surface energy components are relatively small.

Considering the net radiation term, the reduction in the solar flux input comes about because of the increased cloud and surface albedo effects, with an offset due to the increase in input from clear skies (Table 3). The solar effect makes the radiative changes negative, with the largest magnitudes in the domain where the forcing is applied. The increase in the surface longwave flux output is determined by the residual of the downward longwave flux and surface longwave emission, both of which are large and comparable. It results in a small negative value for most of the Northern Hemisphere, with a positive value for land areas near 10°S (Chen 1994), where relatively larger land surface temperature reductions occur (Fig. 4) owing to increased precipitation and soil moisture (section 4).

In LCM, the changes in latent heat flux are less in the midlatitudes (Fig. 13) compared to LLI (Fig. 12), partly due to a lesser radiative forcing. In the southern tropical land region, there is an increase of the latent heat output. The maintenance of the surface energy balance due to the change in each component is approximately similar to that in LLI. However, the balance of fluxes in the ocean area between 20° and 70°N is different in the two experiments, with the net radiative flux in LCM becoming less important than the other terms. This is related to the fact that LLI has perturbation of cloud radiative properties in that region while LCM does not.

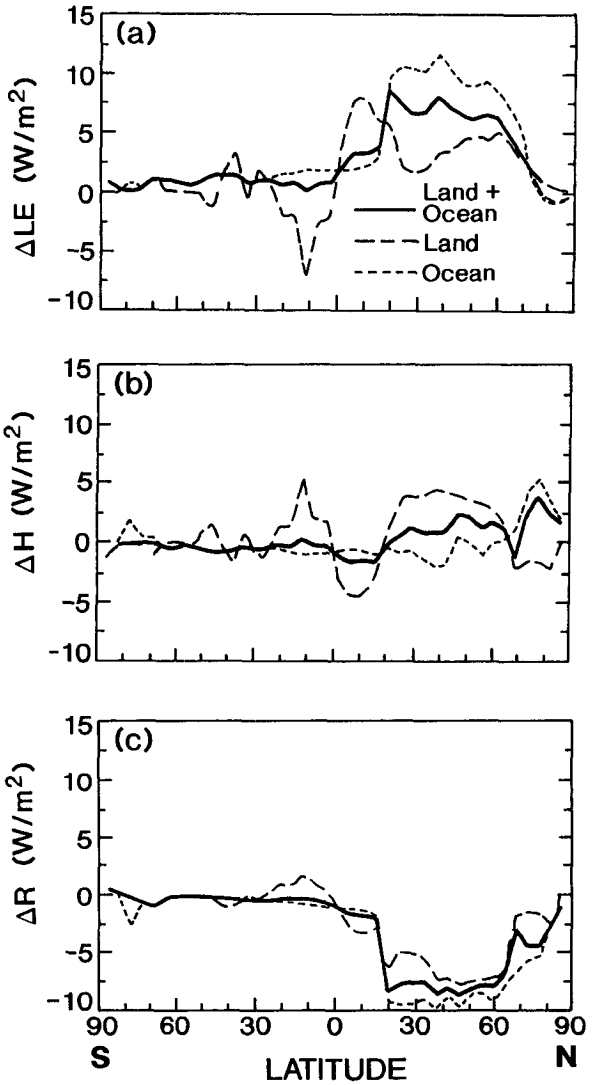

FIG. 12. Zonal, annual-mean distribution of the changes in the land + ocean, land-only, and ocean-only (a) latent heat, (b) sensible heat, and (c) net surface radiative fluxes in the LLI experiment. A positive change acts to warm while a negative change acts to cool the surface.

6. Feedback analyses

The analyses of the feedbacks determining the responses in the LLI and LCM cases is performed following Wetherald and Manabe (1988) and Schlesinger (1989); the procedure is the same as described in

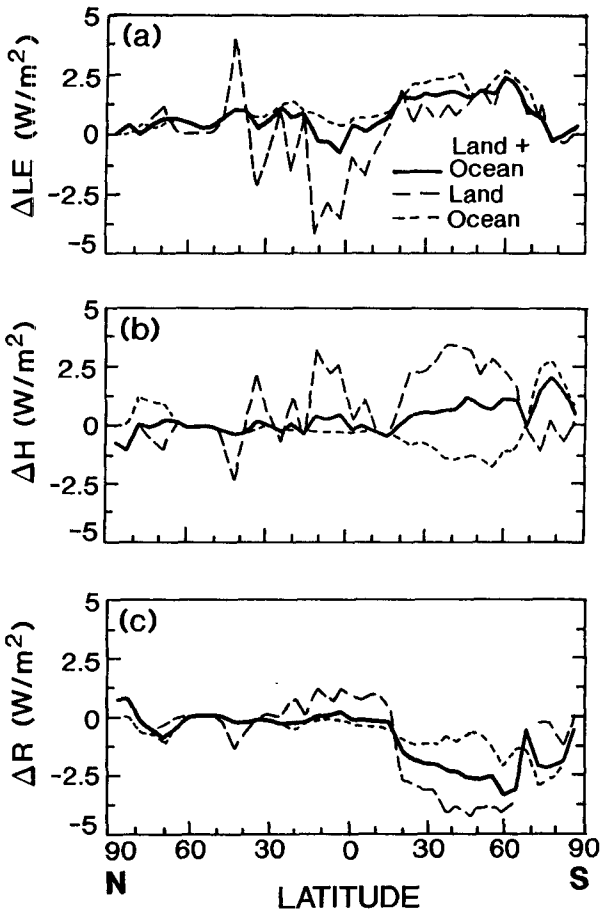

FIG. 13. Same as in Fig. 12 except for the LCM experiment (note the change in scale for the flux changes).

CR96. Because of fixed cloud distributions and properties in the experiments, there is no cloud-related feedback.

Table 4 lists the change in the radiative flux at the top of the atmosphere due to the jth feedback process, $[\delta_j Y]$, as computed for the LLI and LCM experiments (see CR96 for the GLI/2 results). The flux changes are computed separately due to the changes in temperature ($j = T$), water vapor mixing ratio ($j = r$), and surface albedo ($j = A$), as obtained from the GCM simulations (CR96). The changes in the net flux N are subdivided into the shortwave (SW) and longwave (LW) components. The zero feedback gain G_0 is 0.305 K W^{-1} m^2. From Table 4, the net flux changes for $j = T$ and r scale approximately linearly with the global-mean forcing and surface temperature change, similar to that seen for the globally uniform perturbations (CR96).

Table 5 lists the feedback strengths f_j, where f_j is proportional to the change in the radiative flux at the top of the atmosphere due to a change in the jth climate variable per unit global-mean temperature change

TABLE 4. $[\delta_j Y]$ in the different GCM experiments. Units are watts per square meter. SW: net downward solar flux, LW: upward longwave flux, N: net radiative flux at the top of the atmosphere. T, r, and A denote, respectively, temperature, water vapor, and surface albedo change; T_s denotes surface air temperature.

Y	$j = T$	$j = r$	$j = A$
	LLI ($[\Delta T_s] = -1.4$ K)		
SW	−0.1	−0.3	−0.6
−LW	4.4	−1.0	—
N	4.3	−1.3	−0.6
	LCM ($[\Delta T_s] = -0.6$ K)		
SW	−0.1	−0.1	−0.4
−LW	1.9	−0.4	—
N	1.8	−0.5	−0.4
	GLI/2 ($[\Delta T_s] = -1.4$ K)		
SW	−0.1	−0.3	−0.8
−LW	4.4	−1.1	—
N	4.3	−1.4	−0.8

(CR96). The water vapor and surface albedo feedbacks are computed using the data in Table 4. The total feedback $f(\Sigma_j f_j)$ is then obtained by using the radiative forcing (Table 1) and the surface-air temperature response (ΔT_s). As in CR96, we designate the residual of the water vapor and albedo feedbacks from the total as the "lapse rate" feedback, recognizing that a direct computation of this term (e.g., Wetherald and Manabe 1988) may yield a different value. An implicit assumption in the analyses is the additivity of the feedback mechanisms and their independence from each other.

The gain of the climate system with feedbacks, G_f, is also listed in Table 5. The gain links the equilibrium change in temperature to the radiative forcing (i.e., $\Delta T_s = G_f \Delta Q$). Here G_f is quite similar in LLI and LCM (0.74 and 0.78 K W^{-1} m^2). Thus, the total global-mean feedback occurring in each experiment is approximately similar, and the global, annual-mean surface temperature response of the climate system is approximately independent of the spatial characteristics of the radiative forcing applied. More notably, together

TABLE 5. Feedback factor f and the gain of the climate system with feedbacks in the different GCM experiments.

Feedbacks	LLI	LCM	GLI/2
Water vapor	0.29	0.25	0.32
Surface albedo	0.14	0.16	0.18
Lapse rate	0.16	0.20	0.09
Total	0.59	0.61	0.59
Gain of the climate system with feedbacks (K W^{-1} m^2)	0.74	0.78	0.74

with the findings in CR96, whether the forcing is global or spatially confined in the Northern Hemisphere (and even when it is imposed only over the Northern Hemisphere land areas), the global-mean surface temperature sensitivity remains approximately the same. It would thus seem that the global-mean response in T_s is simply related to the global-mean forcing, at least for the types of forcings studied here, with the proportionality constant being the climate sensitivity factor. Note that this factor could differ in value for GCMs with different physics and that the near-invariance feature of the global-mean climate sensitivity masks the differences in the zonal patterns of the climate variables.

In all three experiments listed in Table 5, water vapor feedback is the strongest, consistent with Cess et al. (1990) and the global perturbation cases in CR96. Notwithstanding the above inference regarding the global-mean sensitivity, we do find that the individual processes that contribute to the total feedback reveal important differences. A weaker water vapor feedback in LCM relative to LLI is due to the smaller temperature response in the midlatitude oceanic areas and the smaller changes in water vapor (Fig. 9).

In LLI, the temperature and moisture changes are essentially restricted to the Northern Hemisphere (Fig. 3 and 9a). However, this does not prevent a similarity of the total feedback in LLI and GLI/2 (both have similar global-mean forcings). The water vapor changes in LLI within the Northern Hemisphere midlatitude region (20°–70°N) exceed that in GLI/2 (Fig. 9). However, because of the larger changes in GLI/2 in the low latitudes and their areal extent, the global-mean water vapor feedback exceeds that in LLI. A smaller surface-albedo feedback in LLI relative to GLI/2 is due to the asymmetry in the high-latitude surface albedo response of the two hemispheres. Since the global perturbation experiments with a cooler temperature tend to have a larger surface albedo response in the Southern Hemisphere (CR96), the limitation of the response in LLI to primarily the Northern Hemisphere leads to a somewhat smaller surface albedo feedback. However, because of the greater Northern Hemisphere forcing, LLI does have a relatively stronger effect than GLI/2 in that hemisphere. The larger positive lapse rate feedback in LLI relative to GLI/2 is due to the confinement of the response essentially within the Northern Hemisphere.

In LCM, the total feedback is about the same as GLI/2 and LLI, but it consists of a smaller water vapor feedback and a larger lapse rate feedback than the other two. The smaller water vapor feedback is caused by a lesser reduction in the global water vapor mixing ratio (Fig. 9c). This, in turn, is related to the smaller temperature response in the midlatitude oceanic areas where no radiative forcing was imposed. In section 4, we discussed that the change in ocean evaporation between 20° and 70°N in LCM was negligible but that it is more sensitive in LLI. In LCM, there is also a less enhanced upper-tropospheric cooling (Fig. 6) and therefore less of a negative tropospheric lapse rate feedback. This results in a larger overall positive lapse rate feedback (even relative to LLI) in the surface–atmosphere system. The surface-albedo feedback in LCM is slightly larger than that in LLI. This is due to a relatively larger sea ice change, accompanied by a larger normalized temperature response in the northern polar region (Fig. 7). However, just as in LLI, the localized LCM experiment, too, has a smaller global surface-albedo feedback than GLI/2. Comparing the results for the global and local perturbation cases (CR96 and Table 5), there appears to be a tendency for a compensatory effect in the relative strengths of the different feedbacks so as to yield a near-invariant global-mean climate sensitivity, with the similarity of the climate response arrived at through varying adjustments in the strengths of the various feedback precesses.

7. Summary and discussions

In this study, two GCM simulations have been carried out to investigate the simulated climatic effect of spatially localized perturbations caused by variations or changes in the microphysical property of low clouds. The perturbation is imposed in the midlatitude Northern Hemisphere (20°–70°N) and covers either the entire zone (LLI experiment) or is limited to land areas (LCM experiment). The experiments have relevance to (a) an increase in the albedo of clouds due to anthropogenic sulfate aerosol pollution and (b) the observed contrast in the albedo of land and oceanic clouds. This study complements the globally uniform perturbation experiments in CR96. As in the earlier study, there are no cloud-related feedbacks in the experiments. While the experiments in CR96 were equivalent to global albedo changes, the ones here can be regarded as spatially confined planetary albedo perturbations.

Together with the results from CR96, the global-mean surface temperature response of the model is quite independent of the spatial distribution of the imposed forcing—whether it be globally uniform or spatially localized cloud albedo perturbations or a doubling of the carbon dioxide, that is, the global-mean climate sensitivity (i.e., response to forcing ratio) is nearly invariant for the considered forcings.

However, there are important differences in the zonal-mean thermal and hydrologic responses. The weak interhemispheric heat exchange in the model causes the hemispheric temperature response patterns for the localized perturbation cases to differ from those for the globally uniform cases. For a forcing present only in the Northern Hemisphere, the temperature response is mostly confined to that hemisphere, with only a weak "remote" response in the Southern Hemisphere.

For both global and local perturbations, the temperature change in the tropical upper troposphere exceeds

that in the lower region owing to moist convection. For localized forcings, a strong vertical gradient of temperature change is found in the mid to high latitudes of the Northern Hemisphere where the forcing is applied. In contrast, the lesser temperature response in the Southern Hemisphere is rather uniform throughout the mid and lower troposphere.

With a forcing applied only over the 20°–70°N land area (LCM), there results a nonnegligible temperature response over both oceans and land within this zone. However, scaled to the global-mean response, the oceanic area in the 20°–70°N belt is not perturbed as much as when the forcing is over both land and ocean (LLI). The spatially localized experiments suggest that the observed contrast in drop radii between continental and maritime clouds in the Northern Hemisphere midlatitudes exerts a differential radiative effect over land and ocean areas and thus affects the longitudinal distribution of the surface temperature in this zone.

The relative importance of the individual feedback processes (e.g., water vapor, albedo) is not the same, though the gain of the climate system with feedbacks is very similar for the global and localized perturbation cases. In the latter, the spatial limits of the forcing and temperature response are accompanied by a reduction in the strength of the water vapor feedback relative to the global case. There tends to be a compensation among the different feedback mechanisms such that the total global-mean feedback is nearly the same for all experiments.

A major point of contrast between the globally uniform and the localized perturbation experiments is the temperature response near the equator. In the latter, there is a change in the zonal-mean meridional circulation and moisture transport across the equator. An increase in precipitation occurs just south of the equator due to the strong moisture flux convergence and increased convective activity. There is also a decrease in convective activity between equator and 20°N, which causes a decrease of precipitation there. These features for the localized cases are suggestive of a possible signature of anthropogenic sulfate aerosols (whose forcing is confined to midlatitude northern hemisphere) on climate. It is cautioned, however, that more detailed studies are needed to explore the robustness and strength of these features.

The new surface energy balance for an albedo perturbation applied between 20° and 70°N over both land and ocean areas (LLI) is achieved differently over these two regions. While it is the reduction in the surface latent heat flux that essentially balances the reduction in the solar radiative flux over the ocean, the reduction of the sensible heat flux is more responsible for balancing the solar radiative flux decrease over the continents. When a forcing is applied only over the land areas (LCM) in the same belt, the change in surface evaporation over the midlatitude oceans is less, and sensible heat change also becomes important. There results a smaller ratio of the global-mean precipitation to forcing in the LCM experiment relative to LLI despite a similar global-mean surface temperature sensitivity in the two experiments. This suggests that the contrast in drop radius between maritime and continental clouds, as typified by the LCM experiment, affects the manner in which the surface energy balance is maintained over the land and ocean areas.

The findings here and in CR96 strongly suggest that in the absence of cloud feedback considerations, the global-mean surface temperature response can be simply estimated by computing the global-mean radiative forcing (whether this is due to CO_2, other trace gases, or aerosols). However, the latitudinal distribution of the temperature response, changes in the hydrologic cycle, and alterations in the surface energy budget terms would depend on the spatial characteristics of the forcing.

The conclusions must be considered in the framework of the present study. The localized spatial domain considered here is at least as large as the Northern Hemisphere midlatitude continents. The responses to even more spatially heterogeneous perturbations in cloud microphysical properties, including perturbations over other latitude zones, deserve to be explored. An issue for future studies is why, in both the global and spatially localized experiments, the sum of the feedbacks tends to be the same. The compensatory tendencies in the strengths of the individual feedback components for various types of forcings requires further attention. The manner of representation of various physical processes in the model, such as sea ice, oceanic heat transport, convection and cloud-related (heights, amounts, and properties) feedbacks, and their impacts on the modeled climate response, also need to be critically addressed. It is thus imperative that GCMs be subjected to a number of tests that would enable general conclusions to be reached regarding the global-mean and regional climate sensitivities to inhomogeneous radiative forcings.

Acknowledgments. We thank Drs. L. Donner and A. Robock for many valuable comments and suggestions. We also acknowledge the constructive comments of the anonymous reviewers.

REFERENCES

Boer, G. J., 1993: Climate change and the regulation of the surface moisture and energy budget. *Climate Dyn.*, **8,** 225–239.

Cess, R. D., and Coauthors, 1990: Intercomparison and interpretation of climate feedback processes in 19 atmospheric general circulation models. *J. Geophys. Res.*, **95,** 16 601–16 615.

Charlson, R. J., J. E. Lovelock, M. O. Andreae, and S. G. Warren, 1987: Oceanic phytoplankton, atmospheric sulfur, cloud albedo and climate. *Nature,* **326,** 655–661.

——, J. Langer, H. Rodhe, C. B. Leovy, and S. G. Warren, 1991: Perturbation of the Northern Hemisphere radiative balance by backscattering from anthropogenic sulfate aerosols. *Tellus,* **43AB,** 152–163.

——, S. E. Schwartz, J. M. Hale, R. D. Cess, J. A. Coakley Jr., J. E. Hansen, and D. J. Hofmann, 1992: Climate forcing by anthropogenic aerosol. *Science,* **255,** 423–430.

Chen, C.-T., 1994: Sensitivity of the simulated global climate to perturbations in low cloud microphysical properties. Ph.D. thesis, Princeton University, 279 pp.

——, and V. Ramaswamy, 1995: Parameterization of the solar radiative characteristics of low cloud and studies with a general circulation model. *J. Geophys. Res.,* **100,** 11 611–11 622.

——, and V. Ramaswamy, 1996: Sensitivity of simulated global climate to perturbations in low cloud microphysical properties. Part I: Globally uniform perturbations. *J. Climate,* **9,** 1385–1402.

Erickson, D. J., R. J. Oglesby, and S. Marshall, 1995: Climate response to indirect anthropogenic sulfate forcing. *Geophys. Res. Lett.,* **22,** 2017–2020.

Han, Q., W. B. Rossow, and A. Lacis, 1994: Near-global survey of effective droplet radii in liquid water clouds using ISCCP data. *J. Climate,* **7,** 465–497.

Hudson, J. G., 1984: CCN Measurements within clouds. *J. Climate Appl. Meteor.,* **23,** 42–51.

IPCC, 1992: *Climate Change 1992: The Supplementary Report to the IPCC Scientific Assessment.* Cambridge University Press, 200 pp.

——, 1994: *Climate Change 1994: Radiative Forcing of Climate Change and An Evaluation of the IPCC IS92 Emission Scenarios.* Cambridge University Press, 339 pp.

Jones, A., D. L. Roberts, and A. Slingo, 1994: A climate model study of indirect radiative forcing by anthropogenic sulfate aerosols. *Nature,* **370,** 450–453.

Kiehl, J. T., 1994: Sensitivity of a GCM climate simulation to differences in continental versus maritime cloud drop size. *J. Geophys. Res.,* **99,** 23 107–23 115.

Langner, J., H. Rodhe, P. J. Crutzen, and P. Zimmermann, 1992: Anthropogenic influence on the distribution of tropospheric sulphate aerosol. *Nature,* **359,** 712–716.

Manabe, S., and R. J. Stouffer, 1980: Sensitivity of a global climate model to an increase of CO_2 concentration in the atmosphere. *J. Geophys. Res.,* **85,** 5529–5554.

——, and A. J. Broccoli, 1985: The influence of continental ice sheets on the climate of an ice age. *J. Geophys. Res.,* **90,** 2167–2190.

Penner, J. E., and Coauthors, 1994: Quantifying and minimizing uncertainty of climate forcing by anthropogenic aerosols. *Bull. Amer. Meteor. Soc.,* **75,** 375–400.

Ramaswamy, V., and C.-T. Chen, 1993: An investigation of the global solar radiative forcing due to changes in liquid water path. *J. Geophys. Res.,* **98,** 16 703–16 712.

Rossow, W. B., and A. A. Lacis, 1990: Global, seasonal cloud variations from satellite radiance measurements. Part II: Cloud properties and radiative effects. *J. Climate,* **3,** 1204–1253.

Schlesinger, M. E., 1989: Model projections of the climatic changes induced by increased atmospheric CO_2. *Climate and Geo-sciences: A Challenge for Science and Society in the 21st Century,* A. Berger, S. H. Schneider, and J. Duplessy, Eds., NATO ASI Series C, Vol. 285, Kluwer Academic, 375–415.

Schwartz, S. E., 1988: Are global cloud albedo and climate controlled by marine phytoplankton? *Nature,* **336,** 441–445.

Slingo, A., 1989: A GCM parameterization for the shortwave radiative properties of water clouds. *J. Atmos. Sci.,* **46,** 1419–1427.

Spiro, P. A., D. J. Jacob, and J. A. Logan, 1992: Global inventory of sulfur emission with $1° \times 1°$ resolution. *J. Geophys. Res.,* **97,** 6023–6036.

Squires, P., 1958: The microstructure and colloidal stability of warm cloud. Part II—The causes of the variations in microstructure. *Tellus,* **10,** 262–271.

Twomey, S. A., 1977: The influence of pollution on the shortwave albedo of cloud. *J. Atmos. Sci.,* **34,** 1149–1152.

——, and P. Squires, 1959: The influence of cloud nucleus population on the microstructure and stability of convective clouds. *Tellus,* **11,** 408–411.

——, T. A. Wojciechowski, 1969: Observation of the geographical variation of cloud nuclei. *J. Atmos. Sci.,* **26,** 684–688.

——, M. Piepgrass, and T. L. Wolfe, 1984: An assessment of the impact of pollution on global cloud albedo. *Tellus,* **36B,** 356–366.

Wetherald, R. T., and S. Manabe, 1988: Cloud feedback processes in a general circulation model. *J. Atmos. Sci.,* **45,** 1397–1415.